Physics Program for the STAR/CBM eTOF Upgrade - version 1.3

The STAR/CBM eTOF Group

(Dated: January 14, 2016)

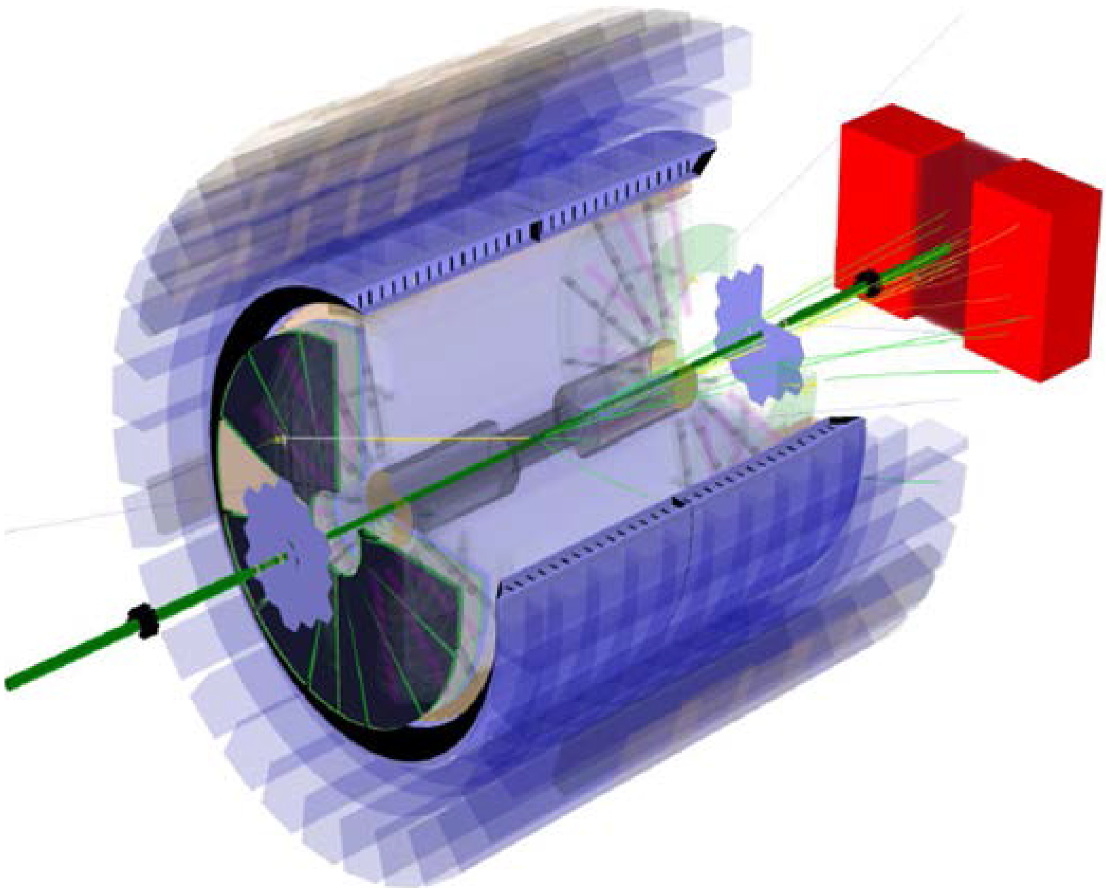

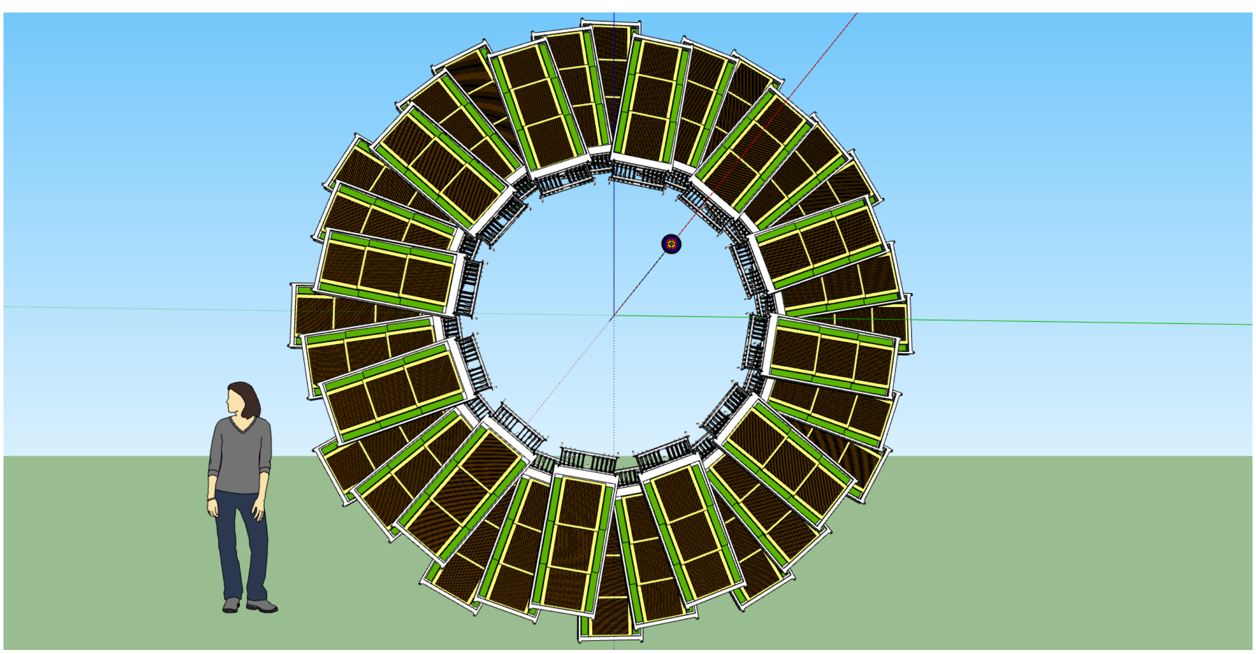

CONTENTS

I. Introduction 2

II. eTOF Improvements to the Physics of the BES Collider Program 3
A. Acceptance 3
B. Rapidity Dependence of p_T Spectra 4
C. Dileptons 5
D. Directed Flow 6
E. Elliptic Flow 7
F. Fluctuations 8

III. eTOF Improvements to the Physics of the Internal Fixed Target Program 8
A. Acceptance 9
B. Energy Range Accessible 10
C. Mapping out the Phase Space 11
D. The Onset of Deconfinement 11
E. Compressibility and the First Order Phase Transition 12
F. Criticality 12
G. Chirality 12
H. Hypernuclei 12

IV. Summary 13

References 13

I. INTRODUCTION

The first RHIC Beam Energy Scan (BES) was an initial survey in which data were acquired from Au+Au collisions at energies of 62.4, 39, 27, 19.6, 14.5, 11.5, and 7.7 GeV in years 2010, 2011, and 2014 [1]. The results from that program have been used to develop a deeper, focused, and refined BES phase II program, which is scheduled to run in years 2019 and 2020 [2]. The BES phase II program relies on low energy electron cooling of RHIC to improve the luminosity [3]. The program focuses on the energy range from 7.7 to 19.6 GeV where the most promising results from the first BES program were seen (energies from 3.0 to 7.7 GeV are accessible through the use of an internal fixed target [4]). Improvements to the STAR detector allow for more refined studies. One of the key upgrades to the STAR detector is the addition of an end-cap Time-of-flight system (eTOF). This detector upgrade allows for particle identification (PID) in the extended psuedorapidty range provided by the iTPC upgrade [5] to the main tracking chamber [6].

The BES phase II program is designed to study the phase diagram of QCD matter (see Fig. 1). The program has several goals:

- Determination of the temperature (T) and baryon chemical potential (μ_B) where the systems created in heavy ion collisions first experience an onset of deconfinement would establish the basic structure of the QCD phase diagram.
- Evidence of the softening of the equation of state consistent with a first-order phase transition is sought to understand the nature of the phase boundary.
- Measurements of enhanced fluctuations, which are the signature of critical behavior, would localize the possible critical point should the phase boundary change from a first-order to a crossover transition.
- Chiral symmetry restoration at high baryon densities, observed through the in-medium modification of the ρ meson mass, would lead to a modification of hadron properties inside nuclei and in hot dense matter.

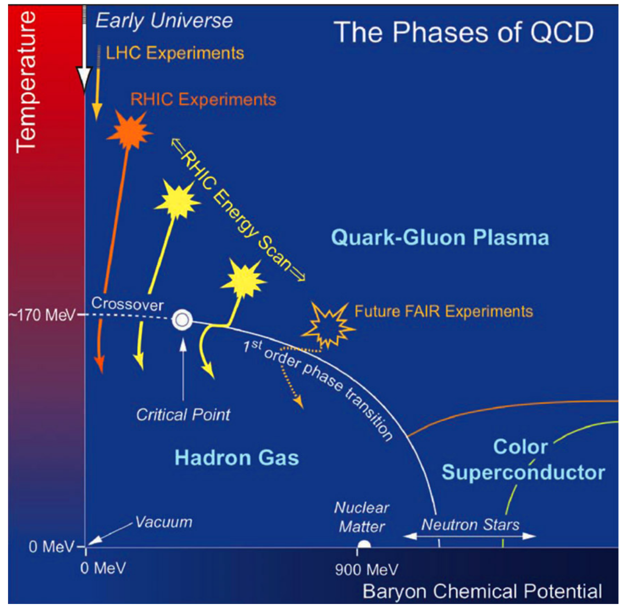

FIG. 1. A conjectured QCD phase diagram with boundaries that define various states of QCD matter [7].

For the collider part of the program, the upgrades extend the pseudorapidity coverage with PID from $|\eta| < 1.0$ to $|\eta| < 1.5$. The eTOF is needed for PID at forward rapidities because the p_Z boost moves the particles beyond the limits of PID through dE/dx. This extended coverage allows for rapidity dependent studies of the key physics observables which is important because the partial stopping of the incident nucleons changes the nature of the system as a function of rapidity. For the internal fixed target part of the program, the role of the iTPC/eTOF upgrades is completely different. In fixed target collisions, the center of mass is boosted in rapidity and the magnitude of this boost is a function of the incident beam energy. For the fixed target program, midrapidity falls inside the main TPC/TOF acceptance window for center of mass energies from 3.0 to 4.5 GeV.

The additional coverage of the iTPC/eTOF is needed for center of mass energies from 4.5 to 7.7 GeV. The iTPC/eTOF upgrades are essential to span this energy gap, thus allowing for a continuous scan from 3.0 to 19.6 GeV combining the fixed target and collider programs of BES phase II.

II. ETOF IMPROVEMENTS TO THE PHYSICS OF THE BES COLLIDER PROGRAM

A. Acceptance

The nature of the improvements to the physics reach of the BES phase II program is dependent on the details of the extended acceptance. There are four key features which are modified by the iTPC and eTOF detector upgrades:

- the low p_T acceptance
- the pseudorapidity coverage
- the dE/dx PID limits
- the TOF PID limits

The transformation Jacobian from pseudorapidity to rapidity is different for each particle species and because different species overlap in different PID spaces, therefore, a separate $y - p_T$ acceptance map must be generated for each particle species: π, K, and p (see Figs. 2, 3, and 4).

The low p_T acceptance limit is the most straight forward. Tracking optimization studies have determined that at least ten hits are needed to identify a track. This criterion was selected in order to reduce combinatoric background and to provide adequate pointing resolution for the tracks to be projected back to the primary vertex. In additional, adequate track sampling length is needed for PID. For the current sector configuration (with short pads in the inner sectors), a track must extend at least five pad rows into the outer outer sectors requiring it to reach a radius of 135 cm, which corresponds to p_T = 125 MeV/c. The iTPC upgrade has more pad rows and longer pads; a track only has to extend 75 cm for a low p_T threshold of 60 MeV/c. These low p_T thresholds are seen at mid-rapidity ($y = 0$) in Figs. 2, 3, and 4).

These same minimum radii can be used to establish the pseudorapidity acceptance of the detector. For the current pad configuration this establishes a maximum of $\eta = 1.2$, while for the iTPC pad configuration the limit is $\eta = 1.7$. By convention, most analysis teams in STAR require at least 25 hits for a *good track*. This criterion requires tracks to reach 170 and 90 cm and this sets the η limits to 1.0 and 1.5 respectively. The barrel TOF system provides coverage to $|\eta| = 1.0$, which corresponds well to the current good track cut. The eTOF system will be mounted at a distance of 270 cm from the center of the detector and will have a radial extent from 100 to 190 cm. This provides coverage of $1.14 < \eta < 1.7$, which leaves a small η gap between the two TOF systems, and will require short tracks to reach the high η limit. These η limits are converted to y using the appropriate transformation Jacobians. These η tracking coverage limits are shown as functions of y and p_T in Figs. 2, 3, and 4.

The dE/dx resolution of gas tracking chambers was empirically studied by Allison and Cobb [8]. Their formula for the percent resolution is:

$$\sigma_{dE/dx} = 0.47 N^{-0.46} (Ph)^{-0.32} \tag{1}$$

where N is the number of samples, P is the pressure in atmospheres, and h is the pad height or length in cm. The outer sectors cover radii from 126-190 cm with 32 pad rows of 1.95 cm pads. The current inner sectors cover radii from 60-120 cm with 13 separated pad rows of 1.15 cm pads. The iTPC inner sectors cover radii from 60-120 cm with 40 pad rows of 1.55 cm pads. From these pad dimensions, one can determine the tracking length for dE/dx and resolution as a function of pseudorapidity. The dE/dx response as a function of momentum for each particle species is given by the Bichsel parameterizations [9]. Using the resolutions and the parametrized response, the momentum limits where pions can no longer be resolved from kaons, and protons can no longer be resolved from pions can be determined. A sample of the relevant values for PID using dE/dx are shown in Table I. These dE/dx PID limits are show as functions of y and p_T in Figs. 2, 3, and 4.

TABLE I. The track lengths, dE/dx resolutions, and p_T limits for PID using dE/dx for various values of η for the current pad plane configuration (TPC), and for the upgraded pad configuration (iTPC).

η	Track Length	$\sigma_{dE/dx}$	π/K (GeV/c)	p/K (GeV/c)
0.0 (TPC)	79 cm	6.8 %	0.80	1.50
0.0 (iTPC)	126 cm	5.5 %	0.82	1.53
0.5 (TPC)	89 cm	6.4 %	0.71	1.34
0.5 (iTPC)	142 cm	5.2 %	0.73	1.36
1.0 (TPC)	91 cm	6.3 %	0.52	0.98
1.0 (iTPC)	163 cm	4.8 %	0.54	1.00
1.2 (TPC)	40 cm	9.3 %	0.42	0.80
1.2 (iTPC)	123 cm	5.5 %	0.45	0.84
1.5 (TPC)	18 cm	13.3 %	0.30	0.59
1.5 (iTPC)	80 cm	6.7 %	0.34	0.54

The PID due to TOF measurements is a function of the timing resolution of the modules and the flight path of the particles. Both the barrel [10] and end-cap [11] TOF modules use the same technology and have the same 80 ps timing resolution. For midrapidity tracks, with a flight path of 2 meters, π/K and p/K separations are achieved for $p < 1.6$ GeV/c and 3.0 GeV/c respectively. These separation cuts scale with an increase in track length. The longest flight path for the barrel TOF are the $\eta =$ 1.0 tracks, which have a path of 2.85 m. The eTOF is set back from the TPC end-cap at a distance of 2.7 m from the interaction point. The longest flight paths for the eTOF are those at η of 1.14, which have paths of 3.3 meters. The shortest paths (2.9 m) are the tracks at $\eta = 1.7$. These TOF PID limits are shown as functions of y and p_T in Figs. 2, 3, and 4.

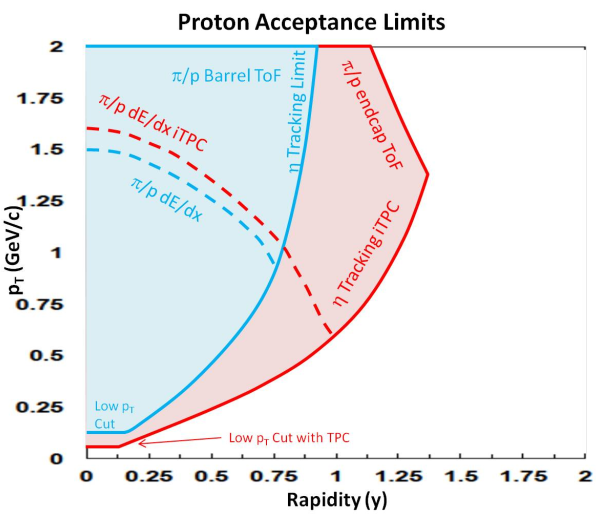

FIG. 2. The $y - p_T$ acceptance map for protons showing the limits due to tracking coverage and PID.

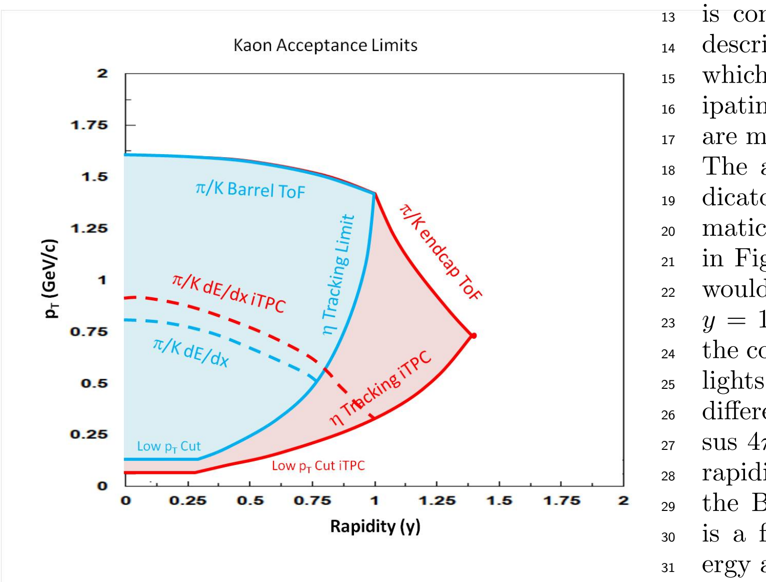

FIG. 3. The $y - p_T$ acceptance map for kaons showing the limits due to tracking coverage and PID.

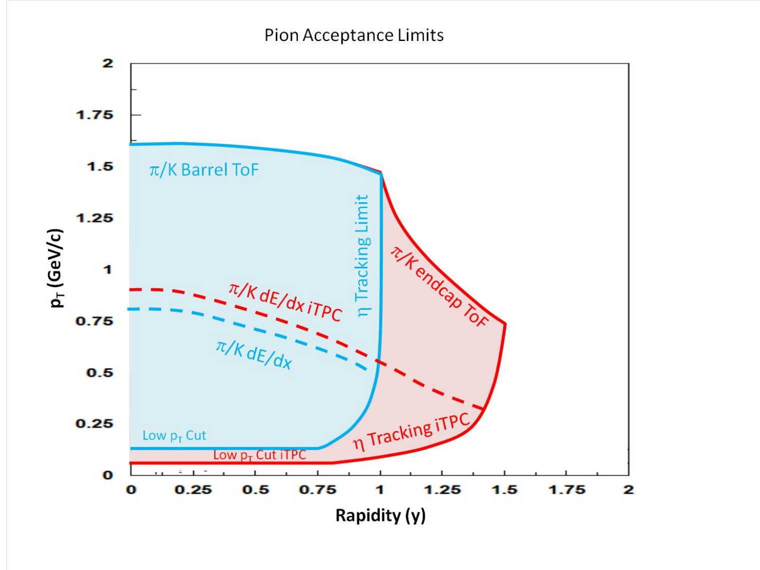

FIG. 4. The $y - p_T$ acceptance map for pions showing the limits due to tracking coverage and PID.

B. Rapidity Dependence of p_T Spectra

At the top RHIC energies and at the LHC, there is a, region of boost invariance at midrapidity, however lower collision energies are characterized by incomplete transparency and partial stopping. This is most readily apparent by comparing the rapidity density distributions of protons to those of anti-protons. Sample distributions are shown in Fig. 5 [12]. The anti-proton yield, which is comprised entirely of produced quarks, can be well described by a Gaussian at midrapidity. The protons, which are comprised largely of quarks from the participating nucleons transported down from beam rapidity, are much flatter and clearly not a thermalized Gaussian. The anti-proton to proton ratio, which is the best indicator of the baryon chemical potential, changes dramatically as a function of rapidity. For the data shown in Fig. 5, the change in the anti-proton to proton ratio would suggest a change in μ_B of 50 MeV from $y = 0$ to $y = 1.2$ (note the magnitude of the change depends on the collision energy). This change in the ratios also highlights why statistical equilibrium models extract quite different T and μ_B values when using midrapidity versus 4π yield data. The figure highlights why this added rapidity coverage, with eTOF PID, is so important for the BES phase II program. As the μ_B of the system is a function of the degree of stopping at a given energy and centrality, it is important that this stopping be measured as directly as possible. In addition, extended rapidity coverage allows for the study of bulk properties as a function of rapidity. The collision energy step size of the BES phase II program was selected in order to measure μ_B steps of about 50-60 MeV; this is roughly the same change in μ_B expected when shifting from $y = 0$ to $y = 1.2$. We should expect to see similar changes in bulk properties when shifting from one BES energy to the next as when shifting from mid to forward rapidity. For $y > 1.0$, the eTOF is required for PID, as seen in Figs. 2, 3, and 4.

Strange baryons and mesons allow one to carefully tease out the stopping of the quarks from the participant

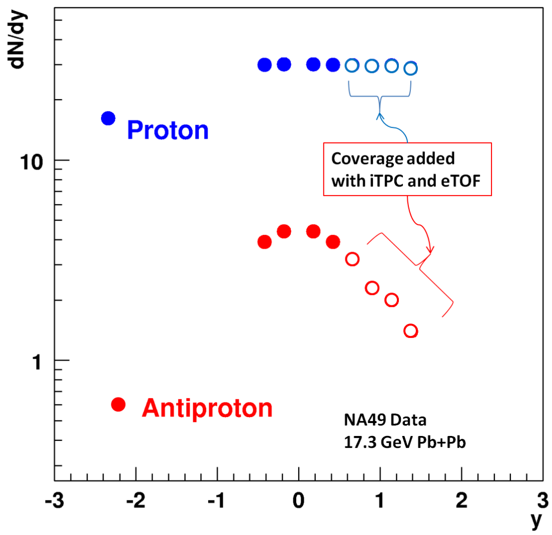

FIG. 5. The dN/dy values for protons from 17.3 GeV Pb+Pb data (circles) are shown [12]. The closed symbols are within the coverage of the current configuration. The open symbols show the extension of coverage which is enabled by the iTPC and eTOF upgrades.

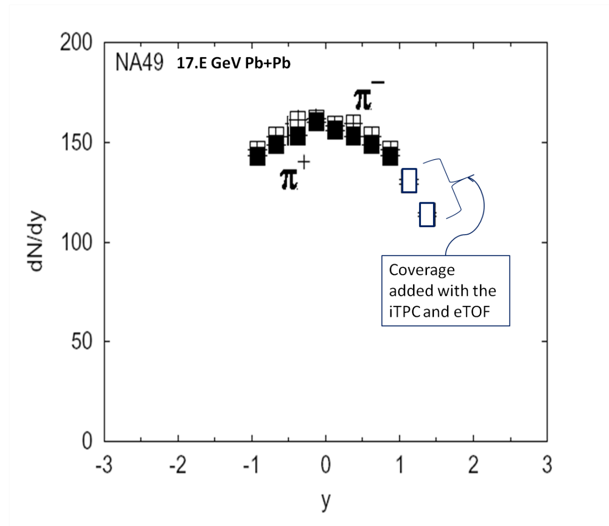

FIG. 6. The dN/dy values for pions from 17.3 GeV Pb+Pb data (squares) are shown [15]. The closed symbols are within the coverage of the current configuration. The open symbols show the extension of coverage which is enabled by the iTPC and eTOF upgrades.

nucleons. The Λ, with one u and one d quark, should show 2/3 of the stopping effects of the proton, while the Ξ^-, with only a single d quark, should show effects at the one third level. The K^+ carries an u quark, while the K^- carries a $\bar{d}$.

The pions are the most copiously produced particles. Although there are some isospin dependent effects at the lowest energies and at very low p_T, the pions are for the most part indicators of the freeze-out surface. The longitudinal extent of the pion rapidity density distribution, compared the width suggested by Landau hydrodynamics, has been used as evidence for a drop in the speed of sound, which is indicative of a first order phase transition [13, 14]. Determining the nature of the phase transition as a function of collision energy is one of the key physics goals of the BES phase II program, and studying the widths of the pion rapidity distributions provides evidence of the expected softening of the equation of state. The capabilities of the STAR detector to measure the pion rapidity density width is illustrated in Fig. 6, where data from NA49 for Pb+Pb collisions is shown [15] in the acceptance window of the current configuration (solid symbols) and with the extended rapidity and PID of the eTOF upgrade (open symbols). In order to determine accurately the width of a Gaussian, the measurement window should be broader than one σ. For the energy range of the BES phase II program, the pion rapidity widths are expected to range from 1.1 to 1.6 units of rapidity as the collision energy increases from 7.7 to 19.6 GeV [16].

C. Dileptons

Studying the decay of short-lived vector mesons into e^+e^- pairs (dileptons) is seen as one of the cleanest probes of the earliest stage of a heavy ion reaction because the daughter electrons escape the colored medium without interacting. The transition from a QGP to a dense hadron gas involves not only a deconfinement transition, but also a spontaneous breaking of chiral symmetry. Chiral symmetry predicts that the spectral functions of chiral partners (ρ and a_1 for example) become degenerate in the symmetric phase. Since it is impossible in heavy ions to measure a spectral function for the $a_1(1260)$ meson, one cannot directly observe the disappearance of the mass splitting between the ρ and $a_1(1260)$ experimentally. Instead, efforts are devoted to studying the modification of vector meson spectral function.

A broadening of the mass of the ρ has been observed from the top SPS energy to the top RHIC energy, which causes an excess in the low mass region (LMR, 200 to 770 MeV/c^2) of the dilepton invariant mass spectrum. Using the broadened ρ spectral function, QCD and Weinberg sum rules, and inputs from Lattice QCD, theorists have demonstrated that when the temperature reaches 170 MeV, the derived $a_1(1260)$ spectral function is the same as the in-medium ρ spectral function, a signature of chiral symmetry restoration. In a model calculation which describes the experimental data, the coupling to the baryons in the medium plays a dominant role in the broadening of the ρ spectral function. The ratio $(p+\bar{p})/(\pi^+ + \pi^-)$, which is a proxy for the total baryon density, remains fairly constant at midrapidity from top

RHIC energies down to the top SPS energy, and then increases as one goes down through the BES phase II range. This predicts a change in the normalized dilepton excess in the LMR of a factor of two from collision energies of 7.7 to 19.6 GeV. As can be seen in Fig.s 5 and 6, one can also change the $(p+\bar{p})/(\pi^+ + \pi^-)$ ratio by a factor of two by shifting the analysis frame from midrapidity to forward rapidity. This rapidity dependence will provide a strong and independent observable to study the total baryon density dependence of the low-mass dielectron emission. Knowing the mechanism that causes in-medium rho broadening and its temperature and baryon density dependence is fundamental to our understanding and assessment of chiral symmetry restoration in hot QCD matter.

Due the high hadron background, experimentally, the quality of the PID is typically the primary limitation for dielectron measurements. Even with iTPC upgrade, the electron identification would still be limited to the pseudorapidity range between ± 1. Electrons are always in the relativistic rise region of dE/dx for gas ionization chambers, and therefore clean PID requires another discriminating measurement such as TOF. With the eTOF upgrade, we can extend the electron identification to the range $|\eta| < 1.5$. Fig. 7 shows the projected BES-II measurements from STAR, with the iTPC, together with data already taken at higher beam energies and compared to recent model calculations. The STAR detector during BES-II will have a unique capability to quantify the total baryon density effect on the rho broadening. The improved measurements during BES-II will enable us to distinguish models with different rho-meson broadening mechanisms; for example, the Parton-Hadron String Dynamic (PHSD) transport model versus Rapps microscopic many-body model with macroscopic medium evolution. The rapidity dependent measurements during BES-II, enabled by the eTOF, will provide complementary information on this important physics topic.

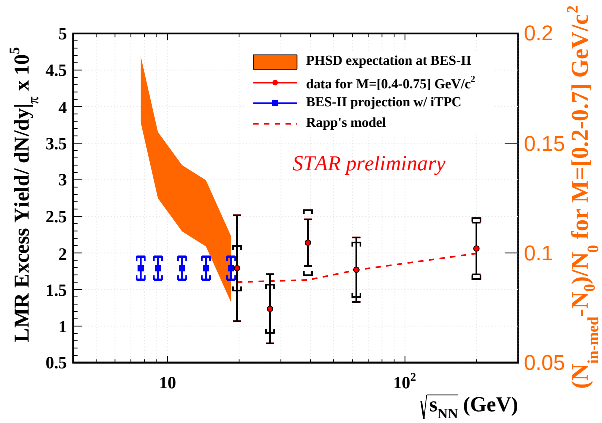

FIG. 7. The Beam Energy dependence for the low-mass dielectron excess from published data at 19.6 [17] and 200 GeV [18, 19], the preliminary results at 27, 39 and 62.4 GeV [20], model expectation from PHSD for energy below 20GeV [21, 22], and Rapps model above 20 GeV [23, 24]. Also shown are projected sys. and stat. errors for BES-II with the iTPC. The bars and boxes represent statistical and systematic uncertainties, respectively.

D. Directed Flow

Proton directed flow (v_1) measurements from the BES-I program have shown a very intriguing and yet unexplained behavior [25]. The midrapidity slope dv_1/dy switches from positive to negative between $\sqrt{s_{NN}} = 7.7$ and 11.5 GeV, and reaches a minimum near 14.5 GeV. The slope dv_1/dy for net protons has a similar minimum but then switches back to a positive slope between 27 and 39 GeV. This could indicate a repulsive compression at the lowest and highest energies, and a softening of the equation of state, consistent with a spinodal decomposition, at the intervening beam energies. Even though this remarkable result stillneeds theoretical reproduction to provide validation, further experimental testscan help elucidate the underlying physics.

During the evolution of a heavy ion collision, gradients of pressures, densities, and temperatures are established across the interaction zone. The lateral edges of the collision will have lower pressure and willbe shifted in rapidity in the direction of the adjacent spectator matter. Thus while we might achieve spinodal decomposition in the center of the collision zone at a particular beam energy, the edge regions might still undergo repulsive compression due to the shifts forward and backward in rapidity. This would in turn affect the $v_1(y)$ slope for protons as a function of rapidity — the so-called wiggle. While the mechanism mentioned above might not be adequate to explain the wiggle phenomenon in its entirety, it is plausible to expect it to modify the wiggle phenomenology and therefore a comprehensive mapping of the $v_1(y)$ structure at BES energies will offer new insights into key details of the QCD equation of state in the relevant region of the phase diagram. NA49 reported some evidence along these lines; seeFig. 8 [26]. However, a much more comprehensive study is needed for conclusive results.

The eTOF will provide proton identification up to a rapidity of 1.2 units, enabling a study of $v_1(y)$ over a new rapidity region for protons, kaons, and pions. Figure 9, based on protons from the UrQMD model at $\sqrt{s_{NN}} =$ 19.6 GeV, illustrates the new parameter space opened up by the eTOF. The $v_1(p_T)$ for three different p_T intervals are shown in the panels of the figure. Guided by the fact that the p_T dependence of every v_n Fourier coefficient is, a priori, of empirical interest (a good illustration of this is provided by constituent quark scaling and its role in QGP discovery, as originally revealed by measurements of $v_2(p_T)$ for mesons and baryons). It is evident from Fig. 9 that the steepening of the proton $v_1(y)$ slope beyond the midrapidity region is not resolvable and thus can not be

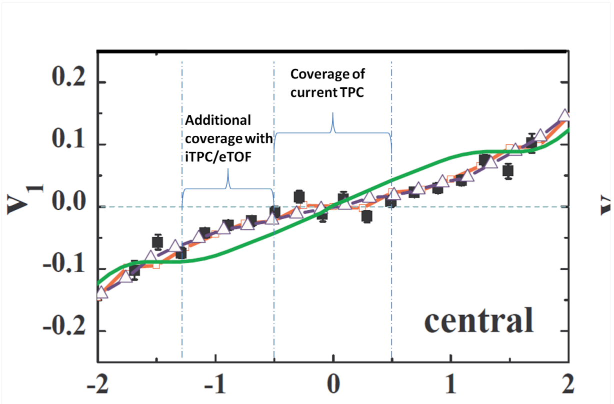

FIG. 8. Directed flow as a function of rapidity for protons from 8.8 GeV (40 A GeV fixed target) Pb + Pb [26].

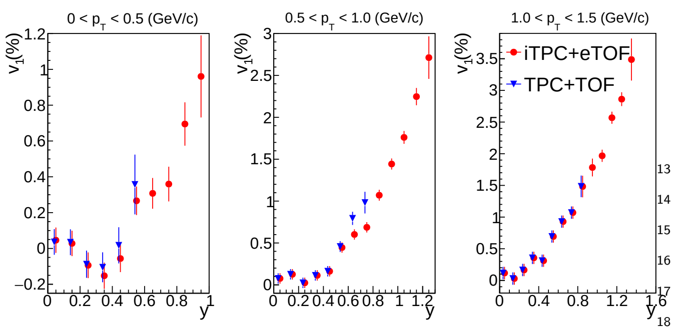

FIG. 9. Proton directed flow as a function of rapidity for minimum-bias Au + Au collisions at $\sqrt{s_{NN}}$ = 19.6 GeV, based on the UrQMD model. The simulated $v_1(y)$ in three intervals of p_T is compared between the acceptance of the STAR TPC with the existing TOF barrel (blue triangles) and the upgraded acceptance after addition of the iTPC and the eTOF (red circles).

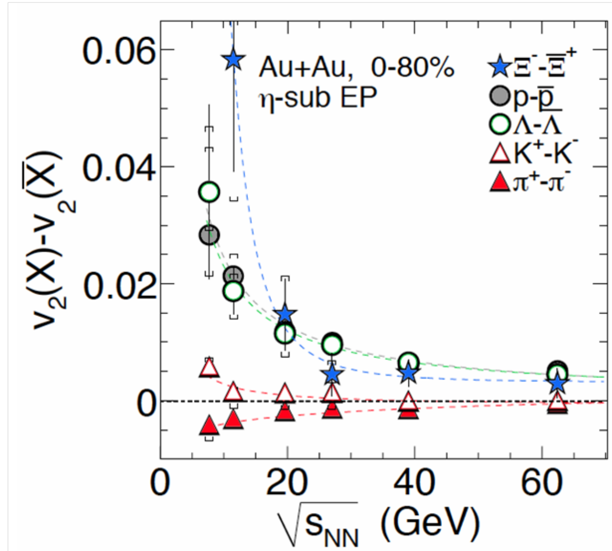

FIG. 10. The measured difference in integrated v_2 between particles and their corresponding antiparticles: pions (filled triangles), kaons (open triangles), Λs (open circles), and protons (filled circles), and Ξs (filled stars) [29].

measured with useful accuracy without the eTOF and iTPC.

E. Elliptic Flow

Number of Constituent Quark scaling (NCQ) of elliptic flow has been seen as one of the cornerstone pieces of evidence that collectivity is established on the partonic level at the top energy of RHIC [27] One of the goals of the BES program is to see how these key QGP signatures evolve with collision energy. Although the quark number scaling of the elliptic flow seems to hold qualitatively for particles and for anti-particles above 19.6 GeV [28] (the statistics are limited below 19.6 GeV), when one compares the v_2 of particles to their respective anti-particles one sees a very different trend as is evidenced in Fig. 10 [29]. This discrepancy could be suggesting a break down in the scaling behavior, or it could be indicating a more subtle effect due to the incomplete transparency and partial stopping of the valence quarks from the participating nucleons. A possible explanation for this behavior is that transported quarks have a very different flow profile from quarks created in the fireball [30]. This conjecture could be tested by studying the elliptic flow at a more forward rapidity where the ratio of transported quarks to created quarks is much higher than that at midrapidity. The particle to anti-particle v_2 differences are expected to increase significantly at $y > 1.0$. The eTOF will enable these rapidity dependent measurements of v_2 which can help us better understand the nature of this QGP signal and whether it either disappears or is simply obscured by other effects as the collision energy is reduced. It is critical that the signatures must be falsifiable. It must be demonstrated that the changes in the signature with energy must be shown to be an effect of QGP physics.

The ϕ meson is a particularly interesting case because it is a meson with the mass of a nucleon. Determining the constituent quark flow behavior of the ϕ meson would be a very sensitive test of whether the flow is established on the partonic level, especially because there is no confounding transported valence quark effect. The results for the flow of the ϕ meson at the lowest energies of the first BES program were suggestive but far from conclusive. This open question is to be answered in the the BES phase II program. However, even with the increased luminosity provided by low energy electron cooling, the v_2 of the ϕ meson is still one of the most statistically demanding measurements proposed for BES II [2]. Since this is one of the top statistics drivers of the program, any upgrade that improves acceptance for the ϕ meson directly improves the program. The ϕ meson is detected through the decay to a K^+K^- pair. The iTPC improves the kaon acceptance at low p_T. The eTOF provides kaon identification up to 1.6 GeV/c in the extended pseudorapidity range $|\eta| < 1.5$.

F. Fluctuations

Net-proton (proxy for net-baryons) and net-kaon (proxy for net-strangeness) kurtosis measurements are likely the best indicators of critical behavior in the vicinity of the the critical point in the QCD phase diagram. We have observed that the net-proton fluctuation signals strongly depend on the p_T and rapidity cuts of the protons (see Fig. 11 [31]). The net-proton fluctuation analyses have used cuts of $0.4 < p_T < 2.0$. Using the current TPC, the rapidity is cut at ± 0.5 ($\Delta y = 1.0$), while with the iTPC, this cut can be extended to ± 0.8 ($\Delta y = 1.6$). Additional particle identification from the eTOF extends the rapidity reach, however, as the rapidity is extended past 0.8, the hard $\eta = 1.5$ acceptance cut imposes a varying low p_T cut-in. This requires a different analysis approach. Instead of plotting the kurtosis as a function of rapidity, it is plotting as a function of the sum of the number of measured protons and anti-protons. This analytical technique is show in Fig. 12 [31]. The STAR BES I data for 7.7 trend upward with total baryons while for 19.6 the trend is downward. It is expected that the kurtosis signal will be large for energies that create systems near the critical point, while for systems with a baryon chemical potential below the critical point the kurtosis will drop below unity. The added coverage of the eTOF will enhance the fluctuation signal providing a clearer and more significant indication of critical behavior.

The addition of the eTOF for PID will have a significant impact on the net-kaon (which is a proxy for net strangeness) and net-charge (which is directly measured from the yields of positive and negative hadrons) fluctuation analyses. The eTOF will allow an extension of the analyses windows for kaons to $y = 1.2$ and for charge to $\eta = 1.5$.

III. ETOF IMPROVEMENTS TO THE PHYSICS OF THE INTERNAL FIXED TARGET PROGRAM

One of the major deficiencies of the BES program at RHIC has been the inability to study collision energies below 7.7 GeV. Although the collider has circulated beams at 5.0 GeV, the drop in luminosity, which is

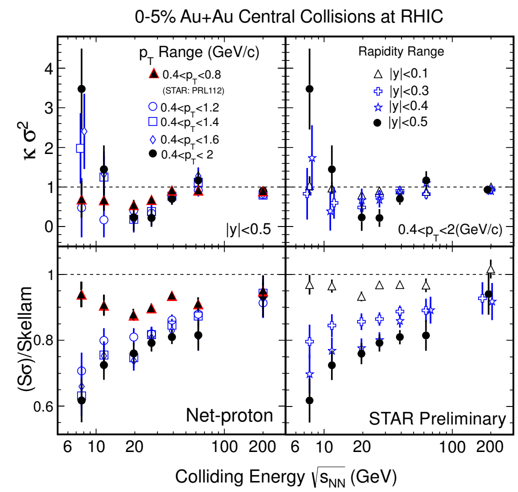

FIG. 11. STAR results for beam energy dependence of $\kappa\sigma^2$ (top panels) and $S\sigma$/Skellam (lower panels) for net-protons in Au+Au collisions [32]. The left panel illustrate the effect of p_T selections while the right panels indicate the effects of rapidity selections. Dotted horizontal lines are expectations from Poisson distributions.

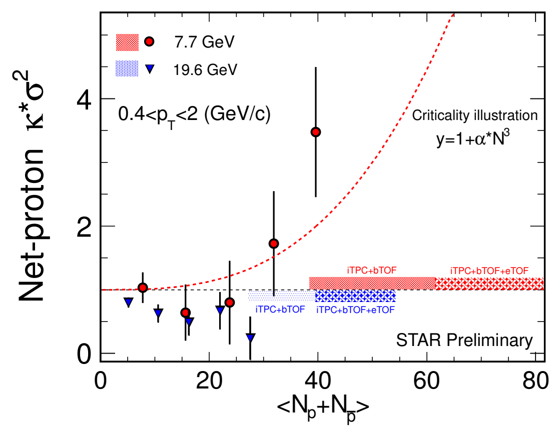

FIG. 12. The net-proton kurtosis as a function of sum of protons and anti-protons.

proportional to γ^3, makes operating below 7.7 GeV impractical. It is important to measure key observables at energies lower than 7.7 GeV for several reasons:

- NA49 has reported that the onset of deconfinement occurs at 7.7 GeV [14]. In order to test this it is necessary to run below this collision energy.

- Some of our QGP signatures (LPV [33] and balance functions [34]) show signs of disappearing at 7.7 GeV. We need to extend the energy range so that we can confirm that these signatures have indeed turned off.

- There are theoretical calculations suggesting that the mixed phase is entered at energies well below 7.7 GeV [35].

The fixed target program at STAR, with the iTPC and eTOF upgrades, addresses this question. Using the current configuration, or even with just the iTPC upgrade, the fixed target program will cover only the cms energy range from 3 to 4.5 GeV. With the eTOF upgrade, we can study the cms energy region 3-7.7 GeV (for those who prefer to quote the projectile kinetic energy per nucleon, this is 3 to 30 AGeV). This allows for a single energy, 7.7 GeV, to be studied in both collider and fixed target modes, which provides important systematic consistency checks. In terms of baryon chemical potential, the five energies of the BES collider program cover the range only from 200 - 420 MeV [36]. With the inclusion of an addition seven fixed target energies, four of which are made possible only with the addition of the eTOF, the range is significantly broader, from 200 - 720 MeV, with a step size of roughly 50 MeV (see Fig. 13). The physics topics proposed for normal collision mode can be performed in this extended μ_B range.

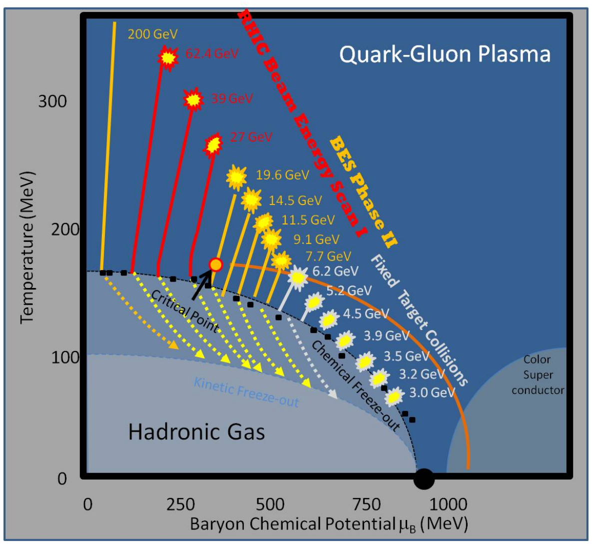

FIG. 13. A schematic of the phase diagram of QCD matter showing the general concepts of the reaction trajectories for the BES collider and fixed target programs.

A. Acceptance

The calculation of the fixed target acceptance of the STAR detector with the iTPC/eTOF upgrades is similar to the collider mode acceptance calculations discussed in the previous section with only a few exceptions. Most importantly, the 1 mm thick gold target is located at $z = +210$ cm in the TPC coordinates. This is the optimal location for the target because it allows measurements from target rapidity to mid-rapidity. The 210 cm shift in the location of the interactions has the following effects on the the acceptance and PID limits of STAR:

- The low p_T threshold value is unchanged. This is affected by the strength of the magnetic field and by the radius of curvature necessary to achieve enough hits for good tracking. An even lower p_T threshold may be optimal for the fixed target program, and this can be achieved by running the STAR solenoid magnet at half of the nominal field, however this optimization is really independent of the detector upgrade configuration, so we will not go into the cost/benefit analysis here.
- The η limits of the detector are changed. In the current configuration, the "short track" limit is $\theta = \arctan(135/410) = 18.2°$ and $\eta = -\ln[\tan(\theta/2)] = 1.83$, while the "good track" limit is $\theta = \arctan(170/410) = 22.5°$ and $\eta = 1.61$. With the iTPC upgrade, the "short track" limit is $\theta = \arctan(75/410) = 10.4°$ and $\eta = 2.40$, and the "good track" limit is $\theta = \arctan(90/410) = 12.4°$ and $\eta = 2.22$.
- The track length in the detector for particles with $\eta > 0.9$ is longer in fixed-target events, therefore, the dE/dx resolutions for these tracks are better then for tracks with similar η values in collider events. A sampling of the dE/dx resolutions is given in Table II.
- The flight path for particles with $\eta > 0.9$ is longer in fixed-target events, therefore, the TOF PID limits for these tracks extend to higher momentum then for tracks with similar η in collider events.

The acceptance and identification limits for fixed target events are shown in Fig.s 14, 15, and 16.

TABLE II. The track lengths, dE/dx resolutions, and dE/dx PID limits for various values of η for the current pad plane configuration (TPC), and for the upgraded pad configuration (iTPC) for fixed target events.

η	Track Length	$\sigma_{dE/dx}$	π/K (GeV/c)	p/K (GeV/c)
0.0 (TPC)	79 cm	6.8 %	0.80	1.50
0.0 (iTPC)	126 cm	5.5 %	0.82	1.53
0.5 (TPC)	89 cm	6.4 %	0.71	1.34
0.5 (iTPC)	142 cm	5.2 %	0.73	1.36
1.0 (TPC)	122 cm	5.6 %	0.53	0.99
1.0 (iTPC)	194 cm	4.5 %	0.54	1.00
1.2 (TPC)	143 cm	5.2 %	0.46	0.85
1.2 (iTPC)	228 cm	4.2 %	0.46	0.86
1.5 (TPC)	186 cm	4.6 %	0.35	0.66
1.5 (iTPC)	296 cm	3.7 %	0.36	0.66
1.7 (TPC)	124 cm	5.5 %	0.29	0.54
1.7 (iTPC)	252 cm	4.0 %	0.30	0.55
1.9 (TPC)	51 cm	8.3 %	0.23	0.43
1.9 (iTPC)	205 cm	4.4 %	0.24	0.45
2.1 (TPC)	38 cm	9.5 %	0.18	0.35
2.1 (iTPC)	174 cm	4.7 %	0.20	0.37

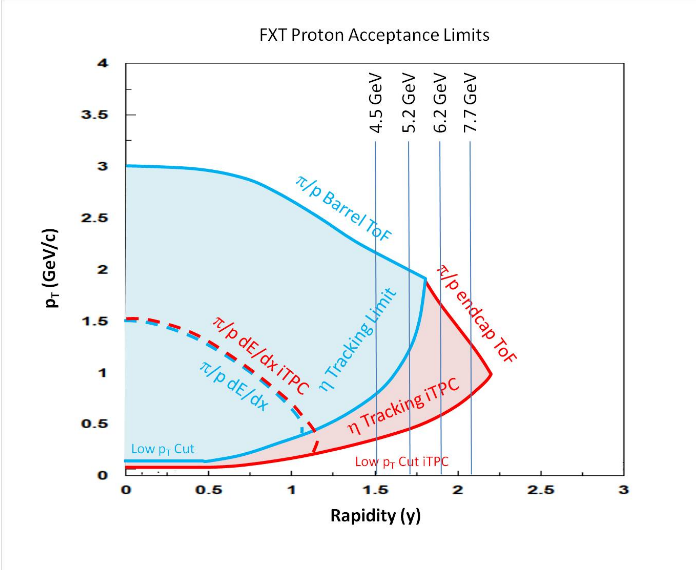

FIG. 14. The $y - p_T$ acceptance map for protons in the fixed target configuration showing the limits due to tracking coverage and PID. The center of mass rapidity lines are shown for the 4.5, 5.2, 6.2, and 7.7 GeV energies.

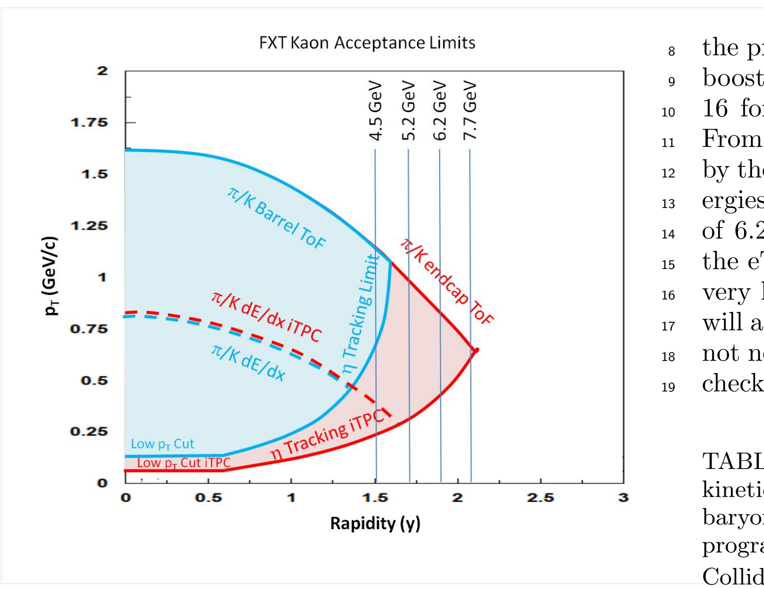

FIG. 15. The $y - p_T$ acceptance map for kaons in the fixed target configuration showing the limits due to tracking coverage and PID. The center of mass rapidity lines are shown for the 4.5, 5.2, 6.2, and 7.7 GeV energies.

B. Energy Range Accessible

In collider mode, the extended η coverage and the PID limits has allowed physics studies at forward rapidities. In fixed target mode, the center-of-mass of the system is boosted in rapidity, therefore the extended coverage of the iTPC and eTOF upgrades affects the range of energies that can be studied. Table III shows a listing of the proposed fixed target energies and the corresponding boosts. The boosts are indicated in Fig.s 14, 15, and 16 for the higher energies of the fixed target program. From these figures, it is evident that the PID provided by the eTOF is needed for kaon and proton studies at energies of 4.5, 5.2, 6.2, and 7.7, and for pions at energies of 6.2 and 7.7 GeV. It should be noted that even with the eTOF PID, studies of protons and kaons will have a very limited range for the 7.7 GeV system. This system will also be studied in the collider program, therefore it is not necessary for all analyses be available for consistency checks.

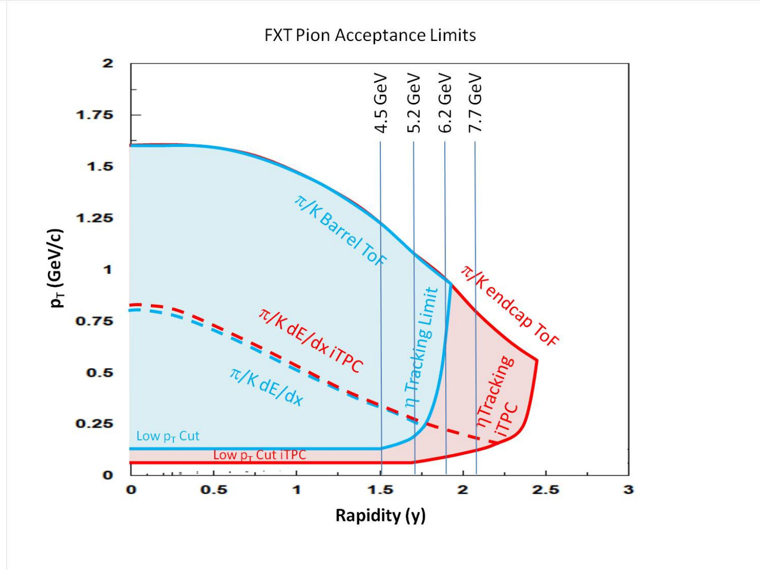

FIG. 16. The $y - p_T$ acceptance map for pions in the fixed target configuration showing the limits due to tracking coverage and PID. The center of mass rapidity lines are shown for the 4.5, 5.2, 6.2, and 7.7 GeV energies.

TABLE III. The center of mass energies ($\sqrt{s_{NN}}$), projectile kinetic energies (AGeV), center-of-mass rapidities (y_{CM}), and baryon chemical potentials (μ_B) for the proposed fixed target program.

Collider	Fixed Target	AGeV	y_{CM}	μ_B
62.4	7.74	30.3	2.10	420
39	6.17	18.6	1.87	487
27	5.18	12.6	1.68	541
19.6	4.47	8.9	1.52	589
14.5	3.90	6.3	1.37	633
11.5	3.53	4.8	1.25	666
9.1	3.20	3.6	1.13	699
7.7	2.99	2.9	1.05	721

Although a detailed proposal for running the fixed target program has not been finalized, the general concept always has been a key part of the BES phase II proposal. Until a more complete proposal is available, we will estimate one day of running at each of the proposed energies. The number of events which can be recorded is limited by

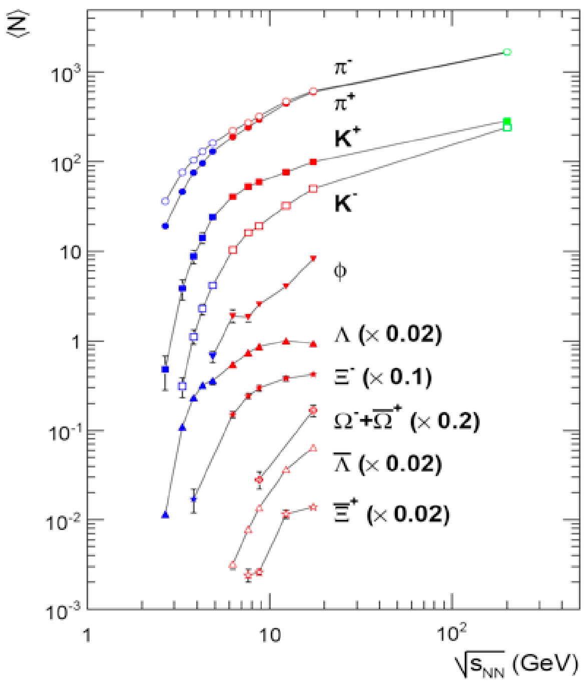

FIG. 17. Yield of mesons, hyperons and anti-hyperons as function of collision energy, measured in central Au+Au or Pb+Pb collisions [37].

the DAQ1000 rate and the expected store length and machine duty cycle. We estimate approximately 50 million events will be recorded at each energy.

C. Mapping out the Phase Space

Exploring the phase diagram of QCD matter requires that at each collision energy we are able to study the yields (both $y_{CM} = 0$ and 4π) of enough species particles to determine accurately the chemical equilibrium T and μ_B values. The coverage maps shown in Fig.s 14, 15, and 16 demonstrate that we have acceptance for π, K, and p from $y_{CM} = 0$ to y_{target} for all fixed target energies except 7.7 GeV, where the K and p acceptances will not be broad enough in p_T for accurate yield measurements. The efficiency for hyperon reconstruction will require a convolution of the single particle acceptances, which still will allow measurement of yields from target to mid-rapidity for K^0_S, Λ, and Ξ^-. Currently, there is only a single Ξ^- measurement in the AGS energy regime. The STAR fixed target program will map out the turn on of Ξ production with collision energy. Measurements of Ω, $\bar{\Lambda}$, and $\bar{\Xi}^+$ have not been made at these energies previously (see Fig. 17); studying the threshold for production of these species could be possible with the fixed target program using the eTOF.

D. The Onset of Deconfinement

NA49 has reported results that are used to suggest that the onset of deconfinement is achieved at 7.7 GeV [14]. This is based on a set of inclusive observables: there is a kink in rate of increase of the pion production with collision energy, there is a step in the slope parameter of the kaon spectra, and there is a peak (horn) in the K^+/π^+ ratio. We will study all of these inclusive observables, in addition the fixed target program will allow us to track the same QGP signature observables that were studied in the first BES program through both the BES phase II collider and fixed target programs. This will be a high precision study of the energy dependence of several observables spanning a collision energy range from 3.0 to 19.6 GeV (μ_B from 720 to 205 MeV). Deconfinement observables which will be studied include:

- The suppression of high p_T particles, as quantified by R_{AA} or R_{CP}, has been seen as the clearest evidence of parton energy loss in a colored medium [38]. The results of the first BES show that the suppression turns into an enhancement at the lower energies. The cause of the enhancement could be either the Cronin effect or radial flow.

- Number of constituent quark scaling of elliptic flow is another key QGP signature [39]. The results from the first BES program show the N_{CQ} scaling is exhibited independently for particles and anti-particles [29]. At fixed target energies the N_{CQ} scaling for particles is expected to break.

- The chiral magnetic effect has been studied with three particle correlators in BES I [33]. For these correlators a discrepancy between the like-sign and unlike sign could be evidence of local parity violation, which would only happen in a deconfined medium. The discrepancy seems to disappear for the 7.7 GeV system. If this explanation is correct, the correlators will continue to show no differences as one studies even lower energies.

- The balance functions are rapidity correlators which should be sensitive to QGP formation. The BES I data show the balance function signal decreases with decreasing beam energy. This signal is almost, but not quite, gone at 7.7 GeV [34]. Lower energy measurements are needed to demonstrate when this signature disappears.

- Strangeness enhancement is seen as an important QGP signature. The energy range covered by the fixed target program sees the opening of several strange particle production channels (see Fig. 17).

E. Compressibility and the First Order Phase Transition

Assuming that there is a first-order phase transition, the concept of a single "onset of deconfinement" is an oversimplification. Depending on the universality class of the phase transition, there may be a spinodal decomposition which would imply a mixed phase region with a negative compressibility. Rather than a single "onset", there may actually be several interesting onsets: the lowest energy which causes some fraction of the system to enter the mixed phase region, the energy at which the system spends the maximum amount of time in the instability regime, and the energy at which the system passes into the pure QGP phase. In order to understand the nature of the phase transition, we propose to study several observables which are expected to have sensitivity to the compressibility. These observables include:

- The directed flow of protons, which offers sensitivity to the early compressibility, as thebulk of these particles are partially stopped participant protons recoiling off the interaction region [25].
- The tilt angle of the pion sources, measured through asHBT [40–42].
- The volume of the pion source, measured through HBT [43].
- The width of the pion rapidity density distribution, which has been shown to be sensitive to the speed of sound in nuclear matter [13].
- The elliptic flow of protons, which has been shown to disappear at a fixed target beam energy of 6 A GeV ($\sqrt{s_{NN}}$ = 3.5 GeV) [44]. This disappearance of v_2 is expected to occur where the transit speed of the projectile nucleus through the target nucleus matches the expansion speed from compression (speed of sound).
- The Coulomb potential of the pion source, which provides an independent means of assessing the source volume, being affected by the expansion velocity of the system [45].

F. Criticality

The observation of enhanced fluctuations would be the clearest evidence that the reaction trajectory of the cooling system had passed near the possible critical end point on the QGP/Hadronic Gas phase boundary. Recent analyses of the higher moments of the net-proton distributions have shown enhanced fluctuations at 7.7 GeV. These results require higher statistics to improve the significance, however in addition to reducing the error bars, an important test to determine if the enhanced fluctuations are related to critical behavior would be to see the fluctuation signals return to their base-line levels at lower energies. The lower energies of the fixed target program would provide for these important control studies. After the improved statistics of the BES phase II program, it may be concluded the the current suggestive results are simply a statistical aberation; in such a case, the lower energy reach of the fixed target program will allow critical behavior searches to be extended to higher μ_B. Although the are some fluctuation analyses performed by the NA49 [46] collaboration, the more refined higher moments studies have been done only by STAR [32, 47] and PHENIX [48] to date. The were no critical fluctuation studies performed at the AGS, so the fixed target program will provide the first such data in this energy regime.

G. Chirality

Di-lepton experiments have been an important part of the physics program at almost all heavy-ion facilities, with the notable exception of the AGS. At the lowest energies (roughly 1.0 AGeV Au+Au), the DLS took data at the Bevalac, while HADES covered a similar energy regime at SIS. In the SPS heavy ion program, dilepton data were taken by experiments Helios-3, NA38/50, CERES, and NA60. And at RHIC, both PHENIX and STAR have dilepton capabilities. The fact that there was no lepton experiment in the suite of AGS experiments means that there are no data in this range. The eTOF detector will provide electron ID at midrapidity for all energies of the fixed target program. This provides the first opportunity to study the evolution of the excess in the LMR in this energy region, in which the low-mass dielectron excess yield might be also sensitive to the temperature in addition to being sensitive to the total baryon density.

In summary, the eTOF upgrade will enable us to measure rapidity-dependence of dielectron excess mass spectra up to $|y| < 1.5$ in the BES-II energy region. It will also enable dielectron measurements at mid-rapidity at the lower energies of the fixed target program. The obtained temperature and total baryon density dependent low-mass dielectron emission will help us to understand the mechanism of in-medium ρ broadening, which is fundamental to probe the chiral symmetry restoration in hot, dense QCD matter.

H. Hypernuclei

The first hyper-nucleus (${}^{3}_{\Lambda}H$) was discovered in 1952, ${}^{4}_{\Lambda}H$ was discovered a little later [49]. Several isotopes of hyper-helium and hyper-lithium have been found in kaon beam s-transfer reactions. In heavy ion collisions, light nuclei are formed through coalescence of nucleons. As the energy is raised nucleons can coalesce with hyperons to form light hyper-nuclei, and at even higher energies

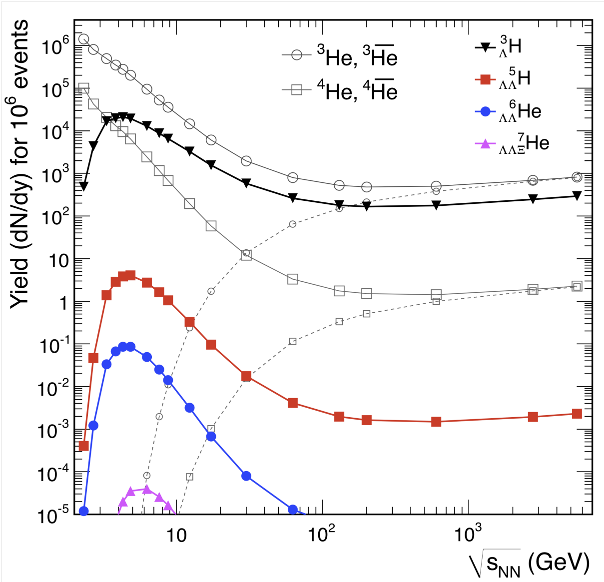

FIG. 18. Energy dependence of hypernuclei yields at midrapidity in Au+Au collisions calculated using the statistical model of [52].

anti-nucleons can coalesce to form light anti-nuclei. This coalescence mechanism has allowed STAR to make the discoveries of anti-hyper-tritium ($^3_\Lambda\bar{H}$) [50] and anti-alpha ($^4\bar{H}e$) [51].

The energy regime covered by the fixed target program (3.0 to 7.7 GeV) should be optimal for the formation of matter (as opposed to anti-matter) hyper-nuclei. At energies below 3.0 GeV, few hyperons are produced whereas at energies above 8 GeV the increased production of anti-baryons stifles matter cluster formation (see Fig. 18). Meaningful samples of $^3_\Lambda H$ and $^4_\Lambda H$ will be measured at all the fixed target energies. Figure 19 shows the expected p_T distribution of hypertritons from a single day of running at 4.5 GeV. The statistics are expected to be comparable to STAR data samples from 200 GeV collider data. These measurements will allow a precise measurement of the light hyper nuclei lifetime and a mapping of the $^3_\Lambda H/(^3He \times (\Lambda/p))$ and $^4_\Lambda H/(^4He \times (\Lambda/p))$ ratios as a function of $\sqrt{s_{NN}}$. Searches for multi-strange hyper nuclei ($^5_{\Lambda\Lambda}H$ and $^6_{\Lambda\Lambda}He$) would make appealing physics goals, however both would likely require more integrated luminosity than is expected for the STAR fixed target program.

IV. SUMMARY

The eTOF upgrade to the STAR detector brings important and compelling new physics to the RHIC BES phase II program. For the core collider mode physics program, the eTOF brings forward PID which is critical for precision studies of the rapidity dependence of key bulk property observables. Because this energy regime is characterized by the incomplete transparency of the participant nucleons (partial stopping), varying the rapidity window of the analyses changes the baryon density and baryon chemical potential in manners similar to changing the beam energy. This additional systematic will further constrain the models and help to clarify the image of the phase diagram of QCD matter. For the internal fixed target program, the additional forward PID capabilities would enable the program to run at collision energies from 4.5 to 7.7 GeV. Without the eTOF, the fixed target program would run at energies from 3.0 to 4.5 GeV only. This would leave a large gap between 4.5 and 7.7. The eTOF allows the energy coverage gap to be closed, making it possible to have a comprehensive scan from 3.0 to 19.6 GeV in $\sqrt{s_{NN}}$ (720 to 200 MeV in μ_B). This energy range spans from regions which are well understood to be compressed baryonic matter up to regions for which partonic behavior is well established.

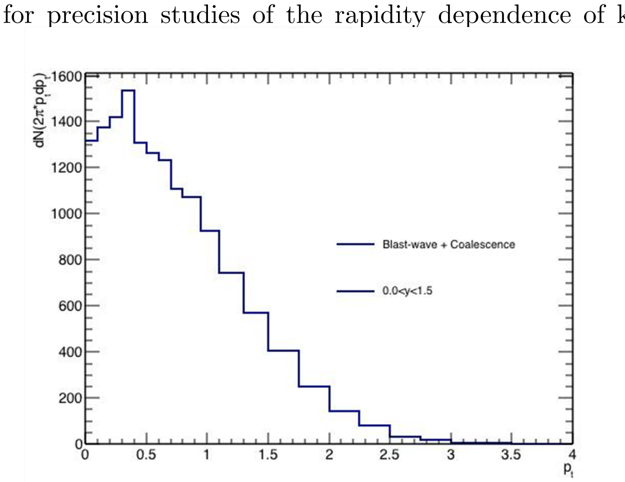

FIG. 19. The simulated p_T distribution of hypertritons from one day of running for fixed target Au+Au collisions at 4.5 GeV.

[1] B. I. Abelev *et al.*, *Experimental Study of the QCD Phase Diagram & Search for the Critical Point: Selected Arguments for the Run-10 Beam Energy Scan*, STAR Internal Note SN-0493 ([STAR Collaboration], 2009).

[2] *Studying the Phase Diagram of QCD Matter at RHIC*, STAR Internal Note SN-0598 ([STAR Collaboration], 2014).

[3] A. Fedotov *et al.*, in *Proc. of Cool09* (2009) pp. 11–15.

[4] S. Collaboration, "A fixed target program for star," In prep.

[5] *A Proposal for STAR Inner TPC Sector Upgrade (iTPC)*, STAR Internal Note SN-0619 (2015).

[6] M. Anderson *et al.*, Nucl. Instrum. Meth. **A499**, 659 (2003).

[7] Picture courtesy of Thomas Ullrich.

[8] W. Allison and J. Cobb, Annual Reviews in Nuclear & Particle Science **30**, 253 (1980).

[9] H. Bichsel, Rev. Mod. Phys. **60**, 663 (1988).

[10] *Proposal for a Large Area Time of Flight System for STAR*, STAR Internal Note SN-0621 (2004).

[11] N. Herrmann, *Technical Design Report for the CBM Time-of-Flight System (TOF)*, GSI Report GSI-2015-01999 (2014).

[12] C. Alt *et al.* (NA49), Phys. Rev. **C73**, 044910 (2006).

[13] H. Petersen and M. Bleicher, *Critical point and onset of deconfinement. Proceedings, 3rd Conference, CPOD2006, Florence, Itlay, July 3-6, 2006*, PoS **CPOD2006**, 025 (2006), arXiv:nucl-th/0611001 [nucl-th].

[14] C. Alt *et al.* (NA49), Phys. Rev. **C77**, 024903 (2008), arXiv:0710.0118 [nucl-ex].

[15] O. Chvala (NA49), *Proceedings, 18th Nuclear Physics Division Conference of the EPS: Phase Transitions in Strongly Interacting Matter (NPDC 18)*, Nucl. Phys. **A749**, 304 (2005).

[16] A. Rustamov, Central Eur. J. Phys. **10**, 1267 (2012), arXiv:1201.4520 [nucl-ex].

[17] L. Adamczyk *et al.* (STAR), Phys. Lett. **B750**, 64 (2015), arXiv:1501.05341 [hep-ex].

[18] L. Adamczyk *et al.* (STAR), Phys. Rev. Lett. **113**, 022301 (2014), [Addendum: Phys. Rev. Lett.113,no.4,049903(2014)], arXiv:1312.7397 [hep-ex].

[19] L. Adamczyk *et al.* (STAR), Phys. Rev. **C92**, 024912 (2015), arXiv:1504.01317 [hep-ex].

[20] S. Yang *et al.*, in *Proc. of QM2015* (2015).

[21] O. Linnyk, E. L. Bratkovskaya, V. Ozvenchuk, W. Cassing, and C. M. Ko, Phys. Rev. **C84**, 054917 (2011), arXiv:1107.3402 [nucl-th].

[22] O. Linnyk, W. Cassing, J. Manninen, E. L. Bratkovskaya, and C. M. Ko, Phys. Rev. **C85**, 024910 (2012), arXiv:1111.2975 [nucl-th].

[23] R. Rapp, Phys. Rev. **C63**, 054907 (2001), arXiv:hep-ph/0010101 [hep-ph].

[24] H. van Hees and R. Rapp, Phys. Rev. Lett. **97**, 102301 (2006), arXiv:hep-ph/0603084 [hep-ph].

[25] L. Adamczyk *et al.* (STAR), Phys. Rev. Lett. **112**, 162301 (2014), arXiv:1401.3043 [nucl-ex].

[26] C. Alt *et al.* (NA49), Phys. Rev. **C68**, 034903 (2003), arXiv:nucl-ex/0303001 [nucl-ex].

[27] J. Adams *et al.* (STAR), Phys. Rev. Lett. **93**, 252301 (2004), arXiv:nucl-ex/0407007 [nucl-ex].

[28] L. Adamczyk *et al.* (STAR), Phys.Rev. **C88**, 014902 (2013), arXiv:1301.2348 [nucl-ex].

[29] L. Adamczyk *et al.* (STAR), Phys.Rev.Lett. **110**, 142301 (2013), arXiv:1301.2347 [nucl-ex].

[30] J. C. Dunlop, M. A. Lisa, and P. Sorensen, Phys. Rev. **C84**, 044914 (2011), arXiv:1107.3078 [hep-ph].

[31] X. Luo (STAR), *Proceedings, 9th International Workshop on Critical Point and Onset of Deconfinement (CPOD 2014)*, PoS **CPOD2014**, 019 (2015), arXiv:1503.02558 [nucl-ex].

[32] .

[33] L. Adamczyk *et al.* (STAR), Phys. Rev. Lett. **113**, 052302 (2014), arXiv:1404.1433 [nucl-ex].

[34] L. Adamczyk *et al.*, "Beam-energy dependence of charge balance functions from au +au collisions at rhic," Submitted Jul. 13, 2015, 1507.03539.

[35] J. Steinheimer and J. Randrup, Phys. Rev. Lett. **109**, 212301 (2012), arXiv:1209.2462 [nucl-th].

[36] J. Cleymans, H. Oeschler, K. Redlich, and S. Wheaton, Phys. Rev. **C73**, 034905 (2006), arXiv:hep-ph/0511094 [hep-ph].

[37] C. Blume, J. Phys. **G31**, S57 (2005).

[38] K. Krajczar (CMS), *Proceedings, 5th International Conference on Hard and Electromagnetic Probes of High-Energy Nuclear Collisions (Hard Probes 2012)*, Nucl. Phys. **A910-911**, 339 (2013), arXiv:1208.6218 [nucl-ex].

[39] J. Adams *et al.* (STAR), Phys. Rev. Lett. **95**, 122301 (2005), arXiv:nucl-ex/0504022 [nucl-ex].

[40] M. A. Lisa, U. W. Heinz, and U. A. Wiedemann, Phys. Lett. **B489**, 287 (2000), arXiv:nucl-th/0003022 [nucl-th].

[41] M. A. Lisa *et al.* (E895), Phys. Lett. **B496**, 1 (2000), arXiv:nucl-ex/0007022 [nucl-ex].

[42] M. A. Lisa, E. Frodermann, G. Graef, M. Mitrovski, E. Mount, H. Petersen, and M. Bleicher, New J. Phys. **13**, 065006 (2011), arXiv:1104.5267 [nucl-th].

[43] M. A. Lisa, S. Pratt, R. Soltz, and U. Wiedemann, Ann. Rev. Nucl. Part. Sci. **55**, 357 (2005), arXiv:nucl-ex/0505014 [nucl-ex].

[44] C. Pinkenburg *et al.* (E895), Phys. Rev. Lett. **83**, 1295 (1999), arXiv:nucl-ex/9903010 [nucl-ex].

[45] G. Baym and P. Braun-Munzinger, Nucl. Phys. A **610**, 286c (1996).

[46] S. V. Afanasiev *et al.* (NA49), Phys. Rev. Lett. **86**, 1965 (2001), arXiv:hep-ex/0009053 [hep-ex].

[47] L. Adamczyk *et al.* (STAR), Phys. Rev. Lett. **113**, 092301 (2014), arXiv:1402.1558 [nucl-ex].

[48] A. Adare *et al.* (PHENIX), (2015), arXiv:1506.07834 [nucl-ex].

[49] Y. Sekido and H. Elliot, "Early history of cosmic ray studies," (D. Reidel Publishing Company, 1985) p. 323.

[50] B. I. Abelev (STAR), Science **328**, 58 (2010), arXiv:1003.2030 [nucl-ex].

[51] H. Agakishiev *et al.* (STAR), Nature **473**, 353 (2011), [Erratum: Nature475,412(2011)], arXiv:1103.3312 [nucl-ex].

[52] A. Andronic, P. Braun-Munzinger, J. Stachel, and H. Stocker, Phys. Lett. **B697**, 203 (2011), arXiv:1010.2995 [nucl-th].